

Article

Hydroclimatic Trends and Drought Risk Assessment in the Ceyhan River Basin: Insights from SPI and STI Indices

Hamid Darabi ¹, Ali Danandeh Mehr ^{2,3,*} , Gülşen Kum ⁴, Mehmet Emin Sönmez ⁴, Cristina Alina Dumitrache ⁵ , Khadija Diani ⁶, Ahmet Celebi ⁷ and Ali Torabi Haghighi ¹ 

¹ Water, Energy and Environmental Engineering Research Unit, University of Oulu, 90014 Oulu, Finland

² Department of Civil Engineering, Antalya Bilim University, 07190 Antalya, Turkey

³ MEU Research Unit, Middle East University, Amman 11831, Jordan

⁴ Department of Geography, Faculty of Arts and Sciences, University of Gaziantep, 27310 Gaziantep, Turkey

⁵ Department of Ecology, Taxonomy and Nature Conservation, Institute of Biology Bucharest, Romanian Academy, 060031 Bucharest, Romania

⁶ LGEE Laboratory, Department of Earth Science, Faculty of Science, Mohammed V- University Agdal, Rabat 10100, Morocco

⁷ Department of Environmental Engineering, Engineering Faculty, Sakarya University, 54050 Sakarya, Turkey

* Correspondence: ali.danandeh@antalya.edu.tr; Tel.: +90-5534178028

Abstract: This study examined the spatiotemporal climate variability over the Ceyhan River basin in Southern Anatolia, Türkiye using historical rainfall and temperature observations recorded at 15 meteorology stations. Various statistical and geostatistical techniques were employed to determine the significance of trends for each climatic variable in the whole basin and its three sub-regions (northern, central, and southern regions). The results revealed that the recent years in the basin were generally warmer compared with previous years, with a temperature increase of approximately 4 °C. The standardized temperature index analysis indicated a shift towards hotter periods after 2005, while the coldest periods were observed in the early 1990s. The spatial distribution of temperature showed non-uniform patterns throughout the basin. The first decade of the study period (1975–1984) was characterized by relatively cold temperatures, followed by a transition period from cold to hot between 1985 and 2004, and a hotter period in the last decade (2005–2014). The rainfall analysis indicated a decreasing trend in annual rainfall, particularly in the northern and central regions of the basin. However, the southern region showed an increasing trend in annual rainfall during the study period. The spatial distribution of rainfall exhibited considerable variability across the basin, with different regions experiencing distinct patterns. The standardized precipitation index analysis revealed the occurrence of multiple drought events throughout the study period. The most severe and prolonged droughts were observed in the years 1992–1996 and 2007–2010. These drought events had significant impacts on water availability and agricultural productivity in the basin.

Keywords: temperature; precipitation; Mann–Kendall; trend; climate change; Ceyhan River



Citation: Darabi, H.; Danandeh Mehr, A.; Kum, G.; Sönmez, M.E.; Dumitrache, C.A.; Diani, K.; Celebi, A.; Torabi Haghighi, A. Hydroclimatic Trends and Drought Risk Assessment in the Ceyhan River Basin: Insights from SPI and STI Indices. *Hydrology* **2023**, *10*, 157. <https://doi.org/10.3390/hydrology10080157>

Academic Editor: Ali A. Assani

Received: 27 June 2023

Revised: 14 July 2023

Accepted: 23 July 2023

Published: 26 July 2023



Copyright: © 2023 by the authors. Licensee MDPI, Basel, Switzerland. This article is an open access article distributed under the terms and conditions of the Creative Commons Attribution (CC BY) license (<https://creativecommons.org/licenses/by/4.0/>).

1. Introduction

Global climate change/variability has an important role in integrated water resources management all over the world [1,2]. Recent climate change and variability studies have highlighted its global significance and the varying impacts experienced across different regions. Consequently, numerous global, regional, and national studies have been conducted to establish evidence of climate change/variability and its implications [3–6]. Similarly, many efforts have been made to monitor and predict extreme climate events such as droughts [7,8]. As Dunn et al. [9] mentioned, climate change/variability is expected to lead to the intensification of the global hydrological cycle, exerting direct influences on overall water resource availability for human and agricultural consumption. Pirnia et al. [10] reported that when precipitation and temperature are varied, streamflow

regimes can change significantly and lead to the appearance of hydrological anomalies such as floods and droughts. They also mentioned climate variability affecting streamflow at a global scale as the most important factor, while at a local scale, human activities such as land use change and dam constructions can affect streamflow. Understanding how climate change/variability might impact both natural ecosystems (such as available water resources) and human society is one of the most sophisticated issues in integrated water resources management [11,12]. Hence, for decades, global and regional climate changes/variability have been widely investigated using different methods and long-term observational data [13–16]. For example, Li et al. [11] used modified Mann–Kendall tests, flow duration curves, and correlation statistics to identify the long-term trend of the hydroclimatological variables. Chong et al. [15] integrated k-means clustering and continuous wavelet transform with Mann–Kendall and sequential Mann–Kendall tests to analyze spatiotemporal variability of meteorological drought events across two Malaysian states. Adu-Prah and Tetteh [16] have assessed relevant information on the role of temperature, rainfall, and humidity on malaria prevalence at different geographic scales for a better understanding of climate variability, and they examined the varying spatial and seasonal distributions in malaria prevalence over time in Ghana. There are similar studies that have investigated spatiotemporal climate variability and its impact on the hydrological cycle and quantity and quality of water resources [17–20].

Given the importance of climate change impacts across the Mediterranean basins, several studies have assessed both short- and long-term changes in hydrometeorological indicators and drought risk in this region (e.g., [21–32]). Focusing on Türkiye, a comprehensive review of drought assessment across the country has been conducted recently [7]. Overall, the study reported an increasing trend in the number of meteorological drought events across the country. Research on agricultural and hydrological drought assessment across the country was also recommended in this study. At the regional scale across Türkiye, the long-term trend of meteorological drought over the Southeastern Anatolia Project (GAP) region was investigated by Gumus et al. [25], indicating a decreasing trend in most of the region. To detect potential trends in meteorological drought events across the capital province of Ankara, 46 years of precipitation and temperature data were used by [26]. Using Spearman rank order and innovative trend analyzing methods, the study showed that the province experienced five extreme drought events during the period 1971–2016. The authors also highlighted a slight descending trend in the observed drought events across Ankara province [26]. The results showed that prolonged severe drought events can correctly be detected by different indices in this region. Eris et al. [27] conducted a comprehensive study on the spatiotemporal variation of drought severity over the Kucuk-Menderes River catchment, western Türkiye. The study compared different site-specific drought indices using historical observations from five meteorological stations to generate drought risk maps for the catchment. More recently, Mersin et al. [28] used long-term precipitation and temperature data from 14 meteorological stations across the Aegean region of Türkiye to investigate drought patterns in the region. The results showed inconsistent drought patterns when different drought indices were derived using the same input variables.

In this study, climate variability across the Ceyhan River basin (Türkiye) was examined for the first time using historical rainfall and temperature observations recorded at 15 meteorology stations during the period 1975–2014. The Ceyhan River basin is already suffering from climate variability [24]. To this end, various statistical and geo-statistical techniques were used to determine the significance of the trends for each climatic variable. In addition, the associated analysis was conducted for the whole basin and three sub-regions (northern, central, and southern regions).

2. Materials and Methods

2.1. Study Area and Data

The Ceyhan River basin is in the central part of Türkiye in the eastern Mediterranean region. The basin with an area of 20,670 km² extends between latitudes of 36°30′–38°42′ and longitudes of 35°30′–38°48′ (Figure 1). The Ceyhan River rises from the Nurhak Mountains of the Eastern Taurus Mountains range at an altitude of 2000–2500 m to the north of the Kahramanmaraş and flows southwest to the Mediterranean Sea near Adana [32]. The Ceyhan River basin is surrounded by the Seyhan basin, the Euphrates in the east and north, the Asi River in the south, and the Seyhan River basin in the west. The basin drains into the Mediterranean Sea in the south. The annual flow of the Ceyhan River is about 7.18 km³, which is equal to 4% of the total streamflow of Türkiye. The 40 years' (1975–2014) rainfall and temperature data from 15 climatology stations inside and around the basin were used to assess the spatiotemporal climate variability over the Ceyhan basin. Table 1 presents the list of climate stations used in this study. To better understand spatial and temporal variation, the basin area and 40 years period were divided into three sub-regions (including northern, central, and southern regions) and four decades (including 1975–1984, 1985–1994, 1995–2004, and 2005–2014). Sub-regions were selected based on their latitude variation (i.e., latitudes of 35.56–36.3, 36.3–38.00, and 38.00–38.71 for southern, central, and northern regions respectively) to cover almost the same change in latitude.

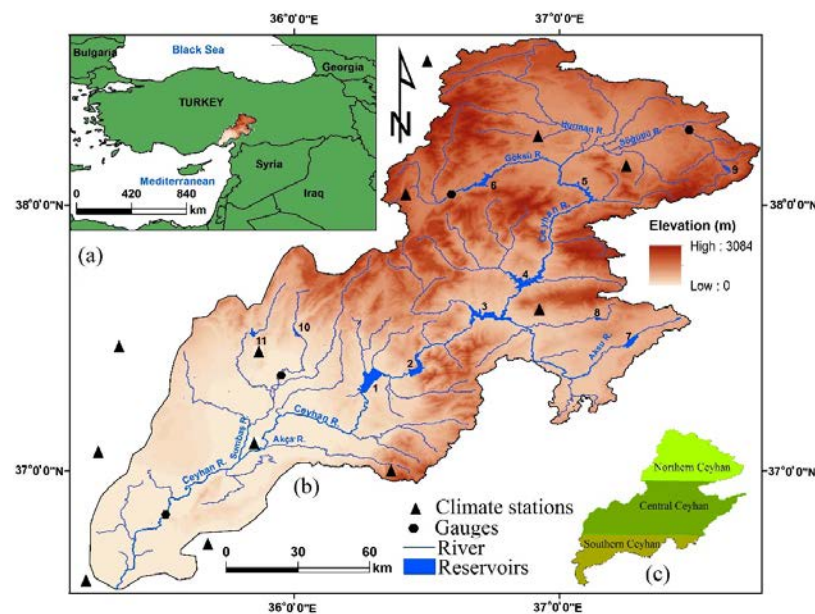


Figure 1. Study area: (a) location of Ceyhan in Türkiye, (b) layout of basin and configuration of climate stations, and (c) three studied sub-regions.

Table 1. List of the climate stations in the study area.

Station	Longitude	Latitude	Mean Annual Temperature (°C)	Mean Annual Precipitation (mm)
Sariz	36.503	39.478	7.46	509.38
Develi	35.479	38.374	11.06	368.43
Pinarbaşı	36.390	38.725	7.77	407.69
Tomarza	35.791	38.452	8.16	395.68
Osmaniye	36.253	37.102	18.52	828.28
Yumurtalik	35.790	36.768	19.12	810.26

Table 1. Cont.

Station	Longitude	Latitude	Mean Annual Temperature (°C)	Mean Annual Precipitation (mm)
Karataş	35.389	36.568	19.16	782.52
Kozan	35.818	37.433	19.46	837.57
Karaisali	35.062	37.250	18.61	882.72
Ceyhan	35.795	37.015	17.99	718.38
Adana	35.298	36.983	19.28	667.64
Afsin	36.919	38.240	10.56	431.71
Elbistan	37.198	38.203	10.90	398.81
Goksun	36.482	38.024	8.93	601.05
Kahramanmaraş	36.915	37.576	16.84	742.74

2.2. Mann-Kendall Test

The Mann–Kendall test as a distribution-free non-parametric method was used to detect significant trends of hydro-climatological time series variables [33–38]. The Mann–Kendall trend test statistic Z is based on Equations (1) to (4).

$$S = \sum_{i=1}^{n-1} \sum_{j=i+1}^n \text{sgn}(x_j - x_i) \quad (1)$$

where x_i and x_j are values in time intervals of i and j , respectively; n is the length of the data set, and:

$$\text{sgn}(\theta) = \begin{cases} +1 & \theta > 0 \\ 0 & \theta = 0 \\ -1 & \theta < 0 \end{cases} \quad (2)$$

If the sample size exceeds ten, the statistic S is nearly normally distributed. The variance of the statistic S ($\text{Var}(S)$) is then calculated as:

$$\text{Var}(S) = \frac{n(n-1)(2n+5) - \sum_t t(t-1)(2t+5)}{18} \quad (3)$$

where t is the extent of any given time, and Σ denotes the summation over the study period.

The values of S and $\text{Var}(S)$ are used to calculate the test statistic, Z , as follows:

$$Z = \begin{cases} \frac{S-1}{\sqrt{\text{Var}(S)}}, & \text{if } S > 0 \\ 0 & \text{if } S = 0 \\ \frac{S+1}{\sqrt{\text{Var}(S)}}, & \text{if } S < 0 \end{cases} \quad (4)$$

where the Z value evaluates the presence of a statistically significant trend. A positive or negative value of Z shows an increase or decrease with time, respectively.

In this study, a MATLAB script was developed for spatiotemporal analysis of the climate variables (rainfall, mean maximum and minimum temperatures at monthly, seasonal, and annual timescales). The basin polygon (Figure 2a) is encompassed by a meshed rectangular grid (Figure 2b). To generate a time series of interpolating functions, the “scattered Interpolant” function (i.e., $F_t = \text{scattered Interpolant}(X, Y, P(t))$) was utilized. This approach was applied to the monthly data from 15 climate stations for each individual time sequence (Figure 2c). For every time instance, the associated value for temperature (or rainfall) was determined by considering the mean value from the mesh cells located within each polygon (Figure 2d).

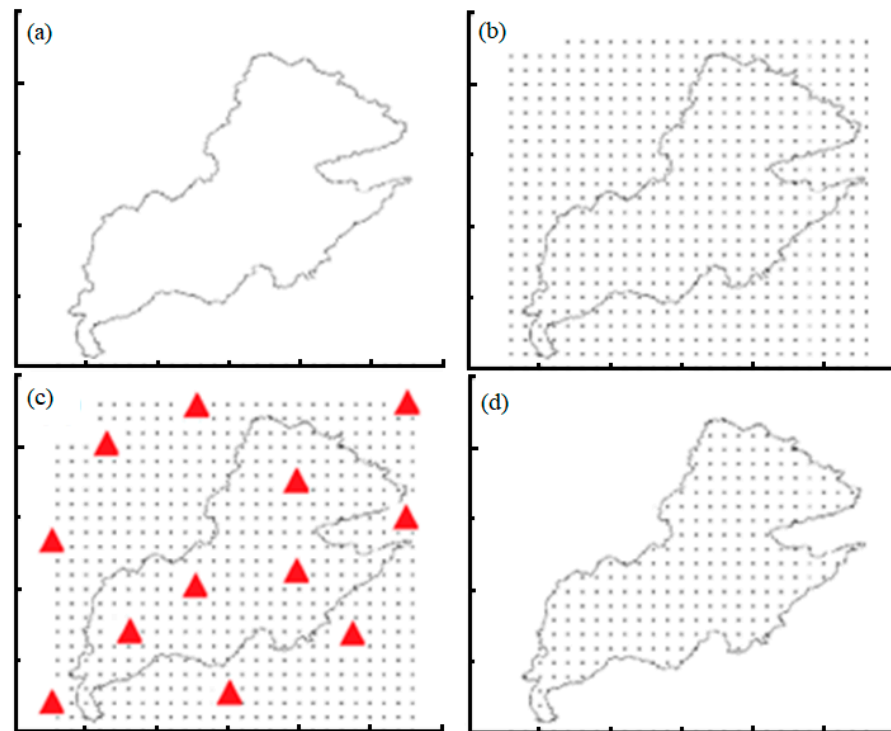


Figure 2. Schematic outline of the process of grid generation within and around the study area based on the geographical location of the observatory stations. (a) basin polygon; (b) rectangular mesh grids; (c) observatory stations; (d) grids located within the polygon.

In this function, X and Y are the longitude and latitude of each of the 15 stations and $P(t)$ is a temporal value of climatic parameters (rainfall or temperature at time t). By applying the function to the data set for each month from 1975–2014, we developed 480 (40 years multiplied by 12 months) functions for monthly rainfall and 480 functions for monthly temperature. Then, by executing F_t to the coordinates of each mesh inside the basin's polygon, the time series of value of P were calculated for each mesh (Equation (5)):

$$P_{(\text{at } X_{\text{mesh}}, Y_{\text{mesh}} \text{ and } t)} = F_t(X_{\text{mesh}}, Y_{\text{mesh}}) \quad (5)$$

Now, a time series of climate parameters (here, rainfall and temperature) is available for each mesh point inside the rectangle, by finding the number of points inside the polygon of the basin. Here, we applied all calculations for four polygons representing the whole Ceyhan basin, the southern, the central, and the northern regions.

In this study, we calculated the spatiotemporal value of rainfall, temperature, standardized precipitation index (SPI), and standardized temperature index (STI). In addition, the trend of each indicator was explored using the Mann–Kendall test for each mesh cell inside the polygons for different time sequences. The selected timing sequences were annual, monthly, two, three, four, five, and six continuous months. Based on these timing configurations, 73 scenarios were developed (1 annual, 12 2-monthlies, 12 2-month, . . . and 12 6-month). To better address the data, monthly time frames were named based on three initial letters of each month (e.g., Jan., Feb., etc.) while other time sequences were named by combining the initial letters of the months. For example, the two-months sequence including January and February is named “JF”, or the name “JFMAMJ” stands for the six-months’ time frame from January to June.

To evaluate extreme events regarding historical temperature records, we classified each time sequence time series based on the STI in seven groups (Table 2):

$$STI_{xy} = \frac{(T_{xy} - \bar{T})}{\sigma} \quad (6)$$

where STI_{xy} is the standardized temperature index for year x and time sequence of y (e.g., JF, JFMAMJ), T_{xy} is the temperature in xy time in year x and time sequence of y , \bar{T} , and σ are the mean and standard deviation for temperature in the selected period. Similar strategies were conducted using rainfall data to develop SPI and evaluate the extreme rainfall events.

Table 2. Thresholds used for STI and SPI classification in this study.

Standardized Precipitation Index (SPI)			Standardized Temperature Index (STI)		
Conditions	Threshold	Color	Conditions	Threshold	Color
Extreme Wet	$SPI \geq 2.5$		Extreme Hot	$STI \geq 2.5$	
Severe Wet	$1.5 \leq SPI < 2.5$		Severe Hot	$1.5 \leq STI < 2.5$	
Mild Wet	$0.5 \leq SPI < 1.5$		Mild Hot	$0.5 \leq STI < 1.5$	
Normal Wet	$0.0 \leq SPI < 0.5$		Normal Hot	$0.0 \leq STI < 0.5$	
Normal Drought	$-0.5 \leq SPI < 0.0$		Normal Cold	$-0.5 \leq STI < 0.0$	
Mild Drought	$-1.5 \leq SPI < -0.5$		Mild Cold	$-1.5 \leq STI < -0.5$	
Severe Drought	$-2.5 \leq SPI < -1.5$		Severe Cold	$-2.5 \leq STI < -1.5$	
Extreme Drought	$SPI < -2.5$		Extreme Cold	$STI < -2.5$	

3. Results

The results of spatiotemporal variations of temperature, rainfall, and their associated trends are discussed in this section.

3.1. Spatiotemporal Variation of Temperature and Hot and Cold Periods

Overall, the thermal view of the basin indicated that the recent years were warmer than earlier years and northern subbasins were colder than southern ones by almost 4 °C. The coldest and warmest years were 1992 and 2010, respectively. The results of the STI analysis show the coldest 1-, 2-, 3-, 4-, 5- and 10-years periods started from 1992, 1992, 1991, 1990, 1989, and 1983, while all the hottest periods started after 2005 (Figure 3). In Figure 3, EC, SC, MC, NC, NH, MH, SH, and EH are abbreviations for the following conditions: extremely cold, severely cold, moderately cold, normal cold, normal hot, moderately hot, severely hot, and extremely hot, respectively [39–41]. Among the first decade of study (1975–1984), only 1979 (15.6 °C) was classified as SH and the STIs for other years were less than 0 and indicated different classes of cold conditions. The percentage of hot years or years with a tendency to hot conditions (class NH) during the second, third, and fourth decades clearly increased to 30%, 70%, and 90%. Surprisingly, in the last decade (2005–2014), only the year 2011 was categorized as MD with a mean annual 14.6 °C (Figure 3a,b); furthermore, the hottest year (2010, 16.7 °C, EH) was also experienced in this period. The temperature distribution was not uniform along the basin for the whole period, and only for 7 years (1976, 1990, 1995, 1999, 2004, 2006, and 2010) were all three regions classified in the same category. The number of years in the middle categories (NC and NH) was 13, about 33% of the period; most of these years (8 out of 13) occurred between 1985–2004. Finally, we can state that among these 40 years, the first decade was quite cold, then during the next 20 years (1985–2004) we observed a transition period from cold to hot in the last decade (2005–2014) (Figure 4).

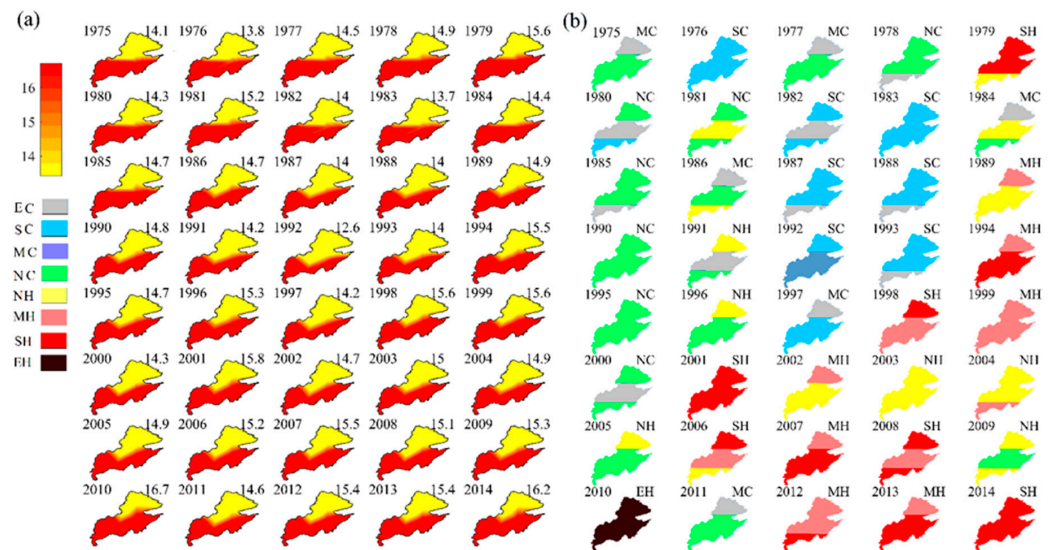


Figure 3. Spatiotemporal variation of temperature in the Ceyhan River basin: (a) mean annual temperature and (b) standardized temperature index.

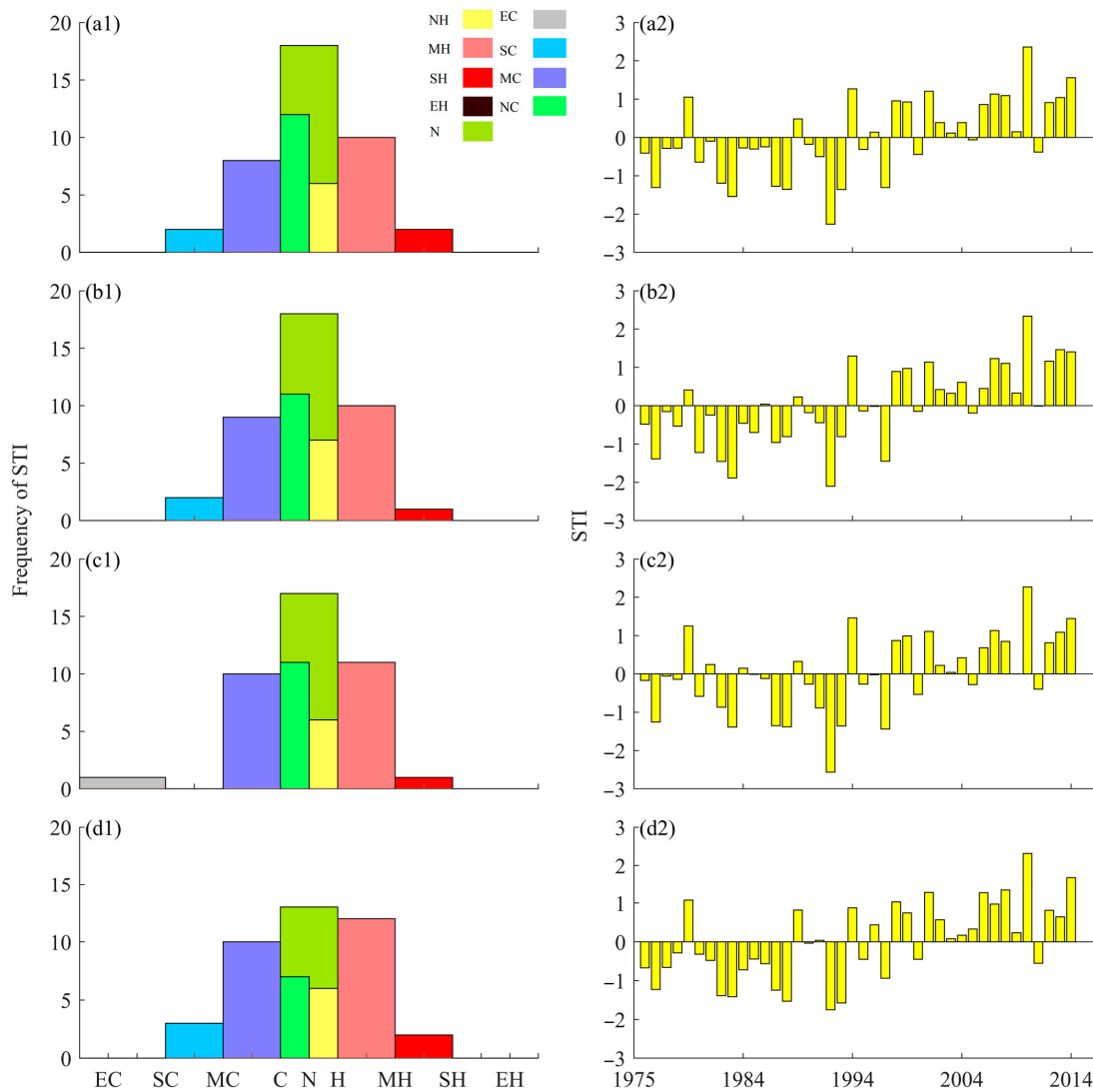


Figure 4. STI variation 1: frequency, 2: annual magnitude in (a): Ceyhan basin, (b): southern, (c): central and (d): northern. N: Normal, M: mild, S: severe, E: extreme, H: hot, C: cold.

3.2. Spatiotemporal Variation of Rainfall

Rainfall distribution in both temporal and spatial scales does not have a uniform pattern across the whole basin. Annual rainfall reduced from the southern to the northern part of the basin. During the period 1975–2014, the mean annual rainfall in the basin was 650 mm; however, in the northern, central, and southern parts, it was 438, 724, and 790 mm respectively (Figure 5). The maximum annual rainfall in the whole basin occurred in 1995, which was similar in the northern and central parts, while in the southern part it occurred in 2009. This issue was also seen for the minimum annual rainfall, which occurred in 2013 in the whole basin, central, and southern parts, but in the northern part, it occurred in 1984. In 27.5% of the studied period (12 years, e.g., 1978, 1981, 1983 and . . .), three different parts of the basin experienced the same rainfall conditions (Figure 5). In Figure 5, EW, SW, MW, NW, ND, MD, SD, and ED are abbreviations for the following conditions: extremely wet, severely wet, moderately wet, normal wet, normal drought, moderate drought, severe drought, and extreme drought, respectively.

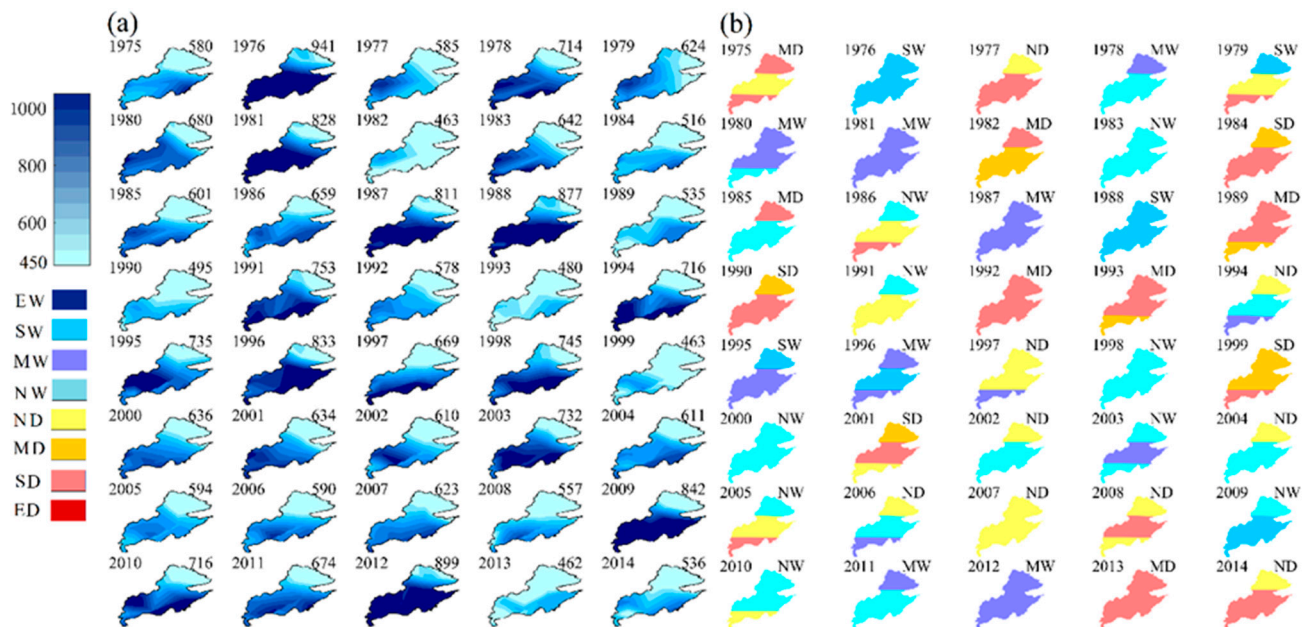


Figure 5. Spatiotemporal (a) rainfall and (b) SPI variability over Ceyhan basin.

Overall, the frequency of dry ($SPI < 0.0$) and wet conditions ($SPI > 0.0$) were almost the same. Normal conditions ($-0.5 < SPI < 0.5$) were most frequent over the Ceyhan and the three regions (Figure 6). In central, south, and the whole basin, the frequency of normal conditions with wet tendency (slight positive SPI, NW, $0 < SPI < 0.5$) was more than normal conditions with drought tendency (small negative SPI, ND, $0 < SPI < 0.5$), while in the northern part the frequency of ND and SD was equal (Figure 6). In the northern part of the basin, the frequency of drought and wet conditions was almost the same. Moderate drought (MD, $-1.5 < SPI < -0.5$) showed most frequency among drought conditions, while normal conditions with wet tendency were most frequent among different wet conditions (Figure 6). The frequency of extreme wet (EW, $SPI > 2.5$) and extreme drought (ED, $SPI < -2.5$) was zero. The northern part frequently had normal conditions with wet and normal drought.

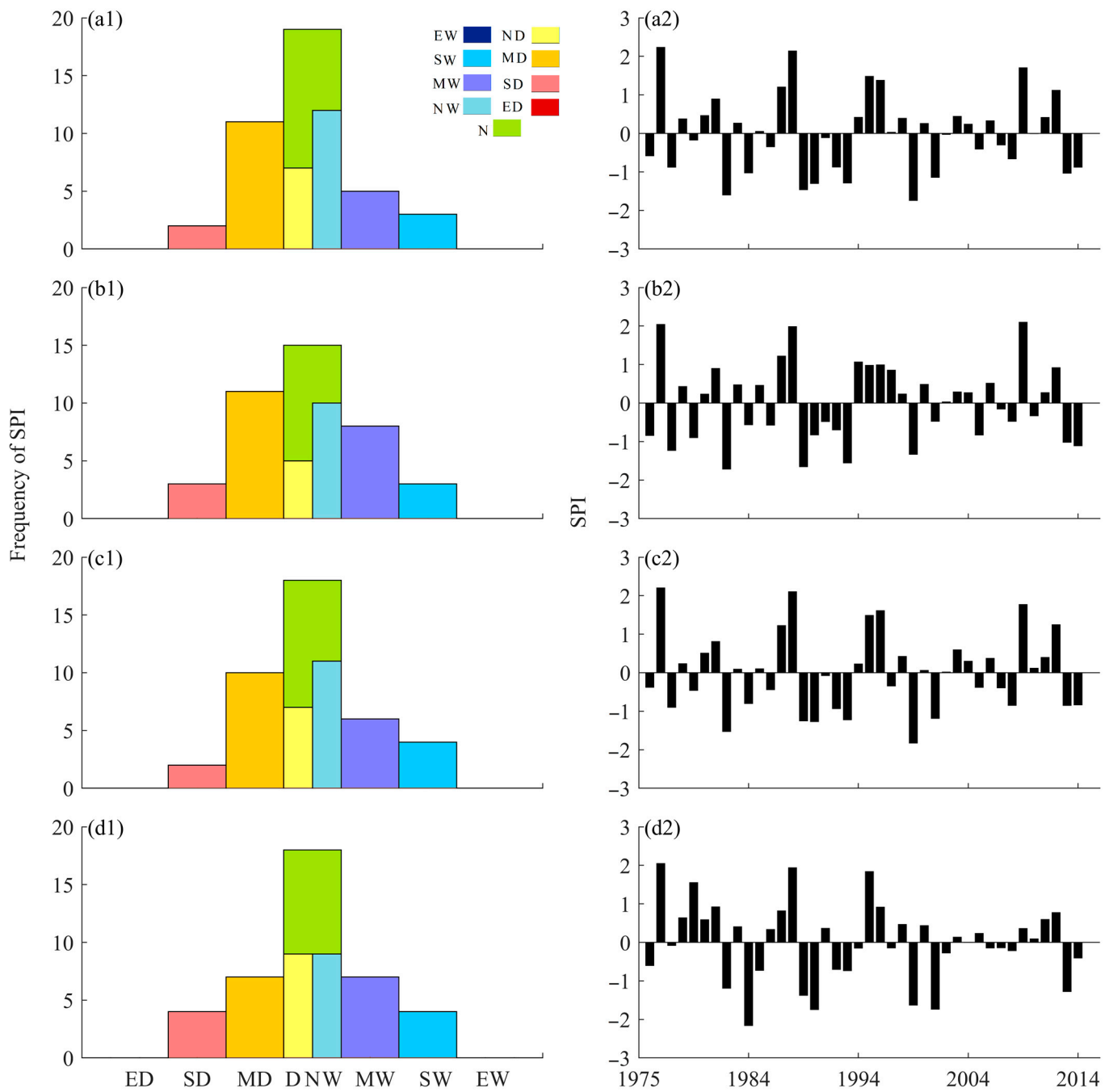


Figure 6. SPI variation 1: frequency, 2: annual magnitude in (a): Ceyhan basin, (b): southern, (c): central and (d): northern. N: Normal, M: mild, S: severe, E: extreme, W: wet, D: drought.

3.3. Trend of Rainfall and Temperature over the Ceyhan Basin and the Sub-Basins

The annual temperature exhibited a significant positive trend across the basin and its three regions, as depicted in Figure 7(a(1)–a(4)). Conversely, the annual rainfall showed only a negative tendency over the basin and three regions, as illustrated in Figure 7(b(1)–b(4)).

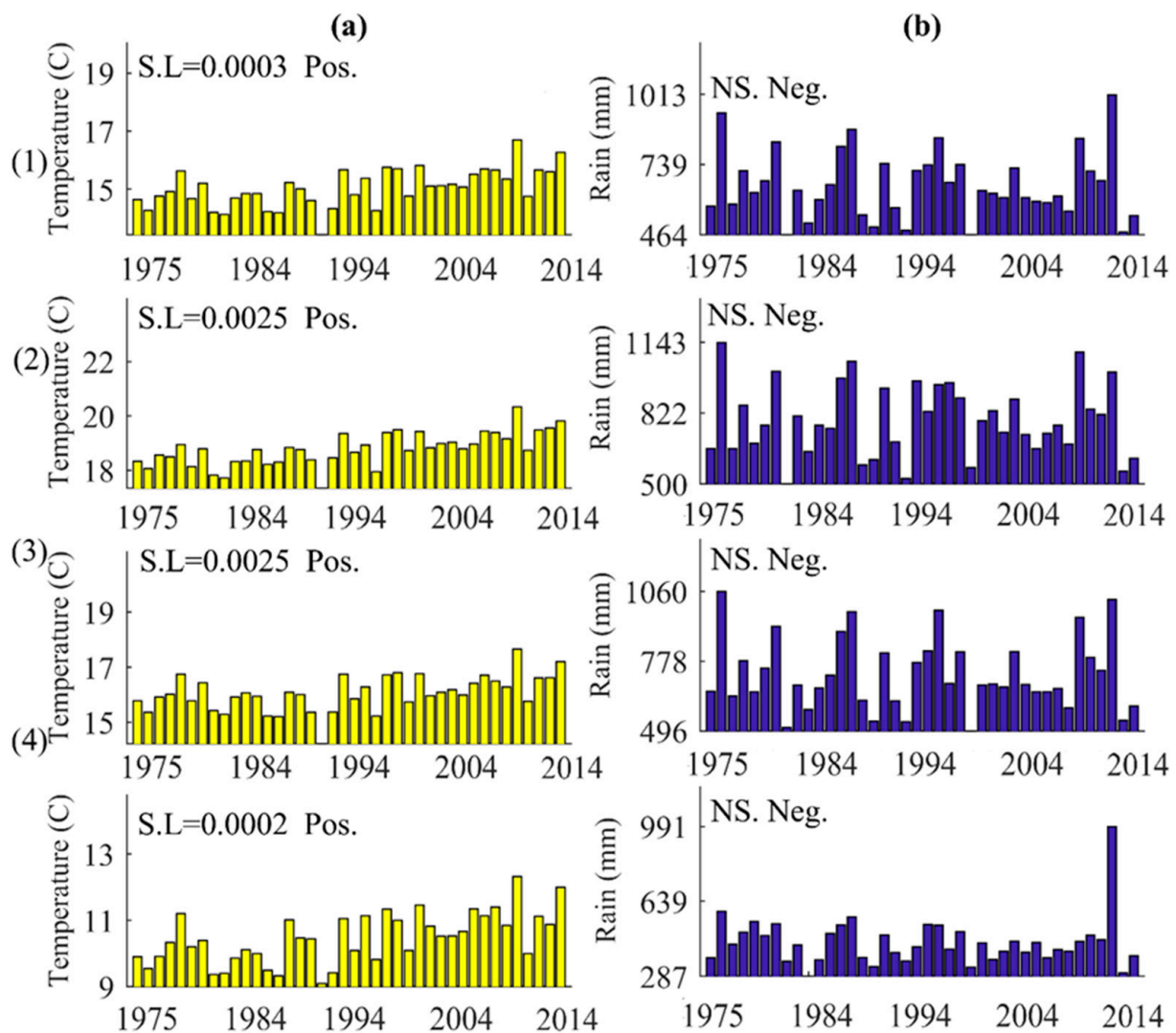


Figure 7. Annual trends of (a) temperature, (b) rainfall over (1) Ceyhan basin, (2) southern, (3) central, and (4) northern parts of the basin. S.L: Significance level, NS.: non-significance, Pos.: positive, Neg.: negative.

Of 73 different scenarios analyzed to assess the intra-annual temperature trend in the entire basin, approximately 44% of the scenarios exhibited a significant positive trend. The remaining scenarios indicated a positive tendency without reaching the threshold for significance (Figure 8(a(1))). Among the monthly time series analyzed, it was observed that the months of June, July, and August exhibited a significant positive trend in temperature. Furthermore, the majority of other scenarios, including those spanning 2, 3, 4, 5, and 6-month periods, also showed a positive trend in temperature (Figure 8(a(1)) and its accompanying footnote). When considering the three regions individually, approximately 58% of scenarios in the southern region, 51% in the northern region, and 18% in the central region demonstrated a significant positive trend in mean temperature for different time periods (Figure 8(a(2)–a(4)), with detailed information provided in their respective footnotes). However, only 3% of rainfall scenarios in the southern region exhibited a significant positive trend, specifically in the months of September and August to September (Figure 8(b(2))), while the remaining scenarios (in all regions and the whole basin) showed either a positive or negative tendency (Figure 8b).

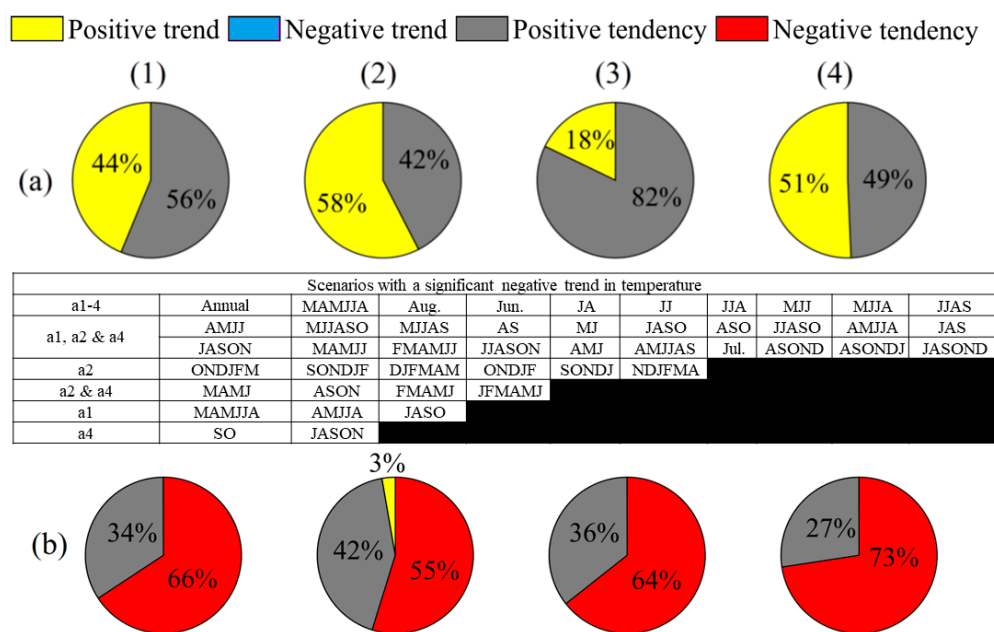


Figure 8. Summarized intra-annual trend of (a) temperature and (b) rainfall for 73 scenarios over the (1) Ceyhan basin, (2) southern, (3) central, and (4) northern parts of the basin. The scenarios with a significant positive trend of temperature (a(1)–a(4)) are mentioned below the figure.

3.4. Intra-Annual Climate Distribution and Variability

Figure 9 provides insights into the changes in temperature (a and c) and rainfall (b and d) across different months of the year in the Ceyhan River basin (1) and its southern (2), central (3), and northern (4) zones. The analysis reveals an overall increase in temperature throughout most months of the year, with a more pronounced rise observed during the warm months of June, July, and August. Furthermore, Figure 9 illustrates the temperature and rainfall patterns for four decades and each month’s contribution to the annual values. Comparing the triple zones of the Ceyhan River basin, it is evident that the southern region experiences higher temperatures compared to the central and northern regions (Figure 9(a2–a4)). Notably, the northern part of the basin exhibits greater temperature variations throughout the months of the year, particularly in comparison to the central and southern regions (Figure 9(a4)). Consequently, the warm months of June, July, and August contribute significantly more to the average annual temperature in the northern region compared with the central and southern regions. In contrast, the temperature differences between months of the year are less pronounced in the central and southern parts of the Ceyhan River basin. For example, in January, the contribution of temperature to the overall annual value is approximately 7% in the southern part, while it is less than 1% in the northern part (Figure 9(b1–b4)).

Regarding rainfall, Figure 9(b1–b4) shows that rainfall occurs throughout the year, with the rainy season typically spanning from October to June. The highest and lowest precipitation rates are observed in January and August, respectively. The contribution of precipitation during July, August, and September is comparatively lower than the other months of the year (Figure 9(a1,d2–d4)). It is important to note that precipitation changes across different months of the year and over the four-decade period do not exhibit regular trends.

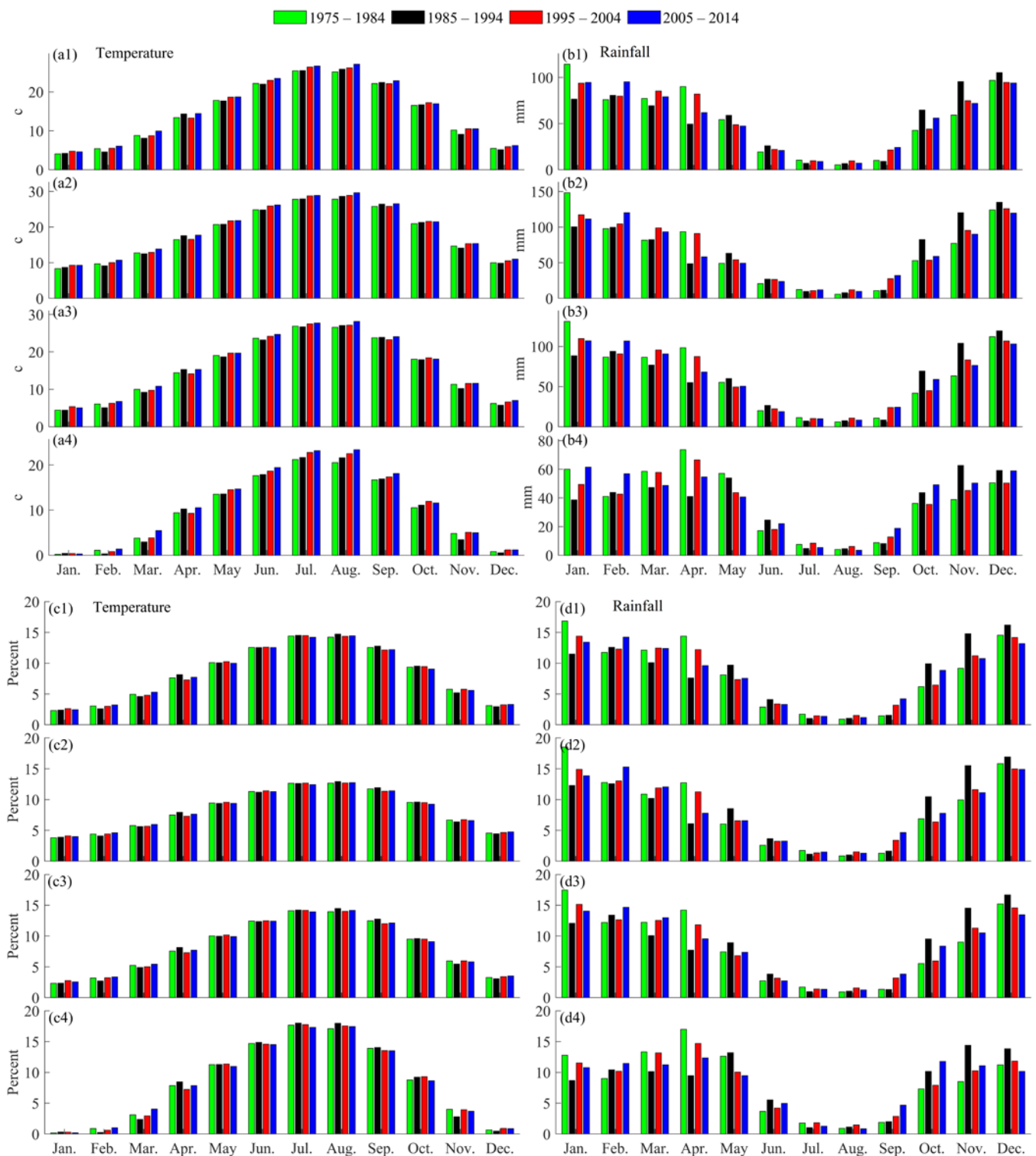


Figure 9. Monthly temperature (a) and rainfall (b) and their distribution (percentage: (c,d) for different decades over the (1) Ceyhan basin, (2) southern, (3) central, and (4) northern part of the basin.

Figure 10 illustrates the monthly variations in temperature and rainfall, comparing the first decade (1975–1984) with the last decade (2005–2014). The overall temperature increase over this period was 0.93 °C, with variations ranging from 0.32 °C in February to 1.99 °C in August. Notably, the highest temperature increases were observed in August (1.99 °C), followed by June (1.3 °C), July (1.21 °C), March (1.14 °C), and April (1.03 °C). August

and July consistently experienced temperature increases across all successive decades (Figure 10a). Regarding rainfall, the second and third decades were characterized by the driest (650 mm) and wettest (667 mm) conditions, respectively. When comparing the first and last decades, the largest increase in monthly rainfall was observed in February (16.6 mm), while the largest decrease occurred in April (−29.1 mm).

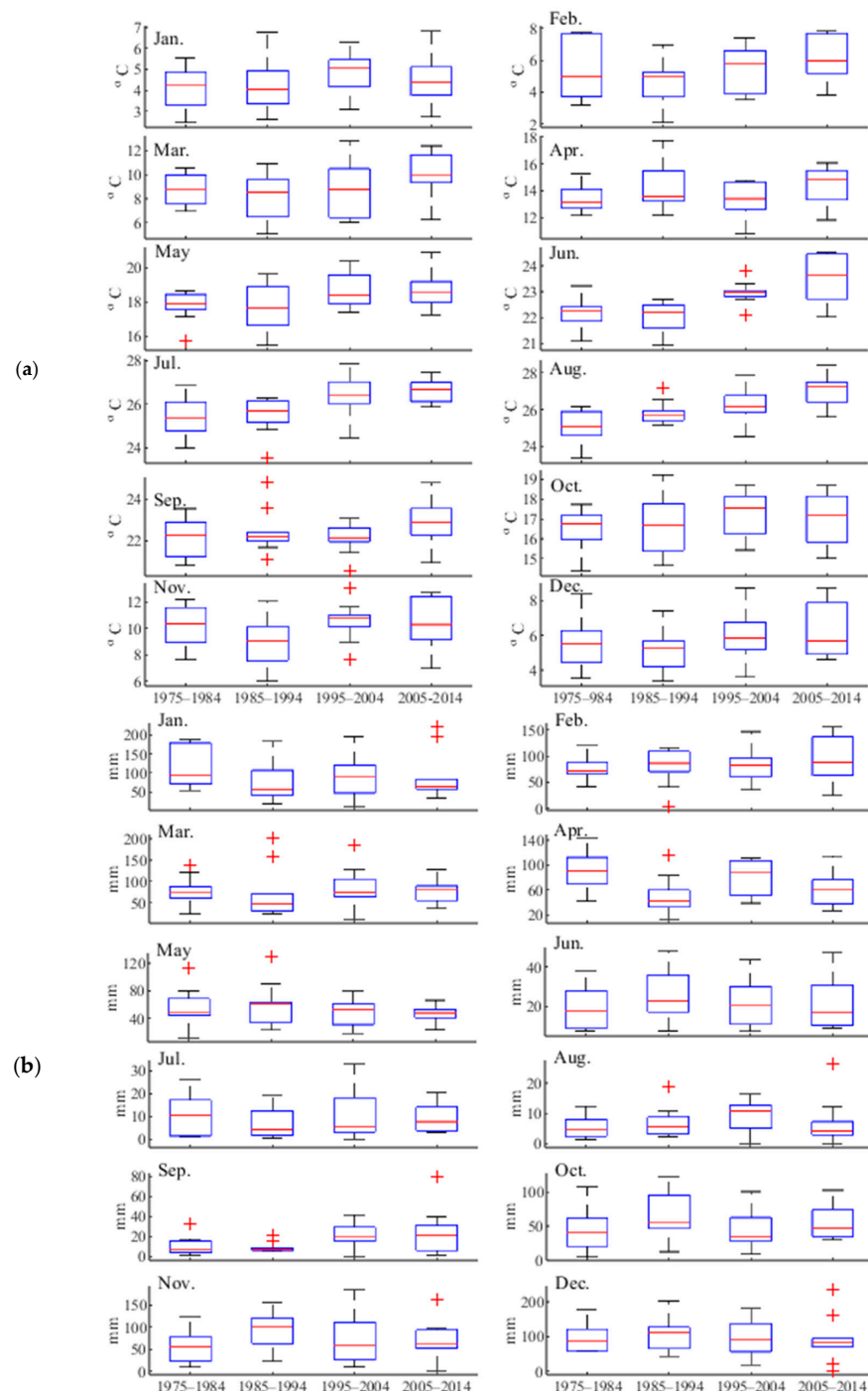


Figure 10. Monthly variability of (a) temperature and (b) rainfall during the different decades.

4. Discussion

The spatiotemporal climate variability over the Ceyhan River basin is described in the results section using historical rainfall and temperature observations recorded at 15 meteorology stations. The results show that the recent years in the basin were generally warmer

compared with earlier years. The coldest and warmest years were identified as 1992 and 2010, respectively. It has been observed that the decrease in temperatures during 1992 can be directly associated with the atmospheric impact of the mount Pinatubo volcanic eruption. This event had a significant effect on the Earth's climate system and caused a decrease in temperature that was evident for several years following the eruption [42]. Over the 40-year period, only seven years exhibited consistent temperature classifications across all three regions. Approximately 33% of the period consisted of years categorized as normally cold and normally hot, with the majority occurring between 1985 and 2004. The results also demonstrated notable fluctuations in rainfall amounts, with both wet and dry periods identified. The wettest year was recorded in 1983, while the driest year occurred in 2008. According to [43], an increasing trend in drought events during the period of 2002–2017 in the Ceyhan River basin has been reported. In addition, the authors demonstrated that Afsin and Elbistan were the driest stations in the Ceyhan basin. This argument supports our finding that the northern part of the basin exhibits greater temperature variations throughout the months of the year, particularly in comparison to the central and southern regions. Furthermore, ref. [24] reported that a strong negative trend in hydrological drought was observed from the early 2000s to 2011 in both the Seyhan and Ceyhan River basins. Regarding rainfall amounts, our study showed that the second period (i.e., 1985–1994) was the driest decade. This implies considerable lag time between meteorological and hydrological dry conditions in the Ceyhan River basin.

5. Conclusions

The impacts of spatiotemporal climate variability on various human activities, such as access to safe drinking water, food production, energy supply, industrial operations, air quality, transportation, sports, and tourism, underscore the importance of integrated water management that considers regional hydrological conditions influenced by climate factors. Previous studies have identified precipitation and temperature as the primary drivers of climate variability affecting the hydrological cycle. In this study, we examined trends and changes in precipitation and temperature over the 1975–2014 period and across four decades using long-term observational data from 15 weather stations in the Ceyhan River basin, encompassing its southern, central, and northern parts. The analysis revealed that rainfall distribution in the basin exhibited a non-uniform pattern both temporally and spatially. Annual rainfall generally decreased from south to north in the Ceyhan River basin, and the spatiotemporal distribution of rainfall in the southern part differed noticeably from the central and northern parts. Additionally, there was a decreasing tendency observed in long-term rainfall variations. On the other hand, the long-term trend and decadal variations of temperature indicated an increasing trend across the Ceyhan River basin, with the northern parts experiencing colder temperatures compared with the southern parts. Assessing the relative contributions of each month to the annual rainfall and temperature, it was found that the warm months of June, July, and August made significant contributions to the overall temperature, accounting for approximately 13% of the total annual amount. In contrast, the contribution of July, August, and September to the overall rainfall was relatively lower compared to other months of the year.

This study was limited to analyzing only ground truth drought across/near the basin, and only meteorological indicators (i.e., SPI and STI) were implemented to detect drought risk. Recent studies have proved the efficiency of satellite data [7] and considering anthropogenic impacts and land use change [9,13] for drought monitoring, prediction, and assessment. Therefore, hydrological indicators for drought assessment and evaluation of the human–water relationship could be considered as topics for future studies. Developing drought resilience plans in the face of increasing water scarcity is also required in practice.

Author Contributions: Conceptualization, A.T.H. and H.D.; methodology, A.T.H., H.D. and A.D.M.; software, G.K., M.E.S., H.D. and A.T.H.; validation, A.T.H., H.D. and A.D.M.; formal analysis, C.A.D., K.D., A.C. and H.D.; investigation, G.K., M.E.S., H.D. and A.T.H.; resources, G.K., M.E.S. and A.D.M.; data curation, G.K., M.E.S. and C.A.D.; writing—original draft preparation, A.T.H. and

H.D.; writing—review and editing, A.T.H., H.D. and A.D.M.; visualization, A.T.H., H.D. and A.D.M.; supervision, A.T.H. All authors have read and agreed to the published version of the manuscript.

Funding: This research received no external funding.

Data Availability Statement: Data are available upon request.

Acknowledgments: We are thankful for the anonymous reviewers for their constructive comments.

Conflicts of Interest: The authors declare no conflict of interest.

References

- Dams, J.; Nossent, J.; Senbeta, T.B.; Willems, P.; Batelaan, O. Multi-model approach to assess the impact of climate change on runoff. *J. Hydrol.* **2015**, *529*, 1601–1616. [[CrossRef](#)]
- Adu-Prah, S.; Appiah-Opoku, S.; Aboagye, D. Spatiotemporal evidence of recent climate variability in Ghana. *Afr. Geogr. Rev.* **2019**, *38*, 172–190. [[CrossRef](#)]
- Amin, M.Z.M.; Shaaban, A.J.; Ercan, A.; Ishida, K.; Kavvas, M.L.; Chen, Z.Q.; Jang, S. Future climate change impact assessment of watershed scale hydrologic processes in Peninsular Malaysia by a regional climate model coupled with a physically based hydrology model. *Sci. Total Environ.* **2017**, *575*, 12–22. [[CrossRef](#)] [[PubMed](#)]
- Mogano, P.; Mokoele, N. South African Climate Change Adaptation Politics: Urban Governance Prospects. *Int. J. Humanit. Soc. Sci.* **2019**, *11*, 68–83.
- Madzivhandila, T.S.; Niyimbanira, F. Rural economies and livelihood activities in developing countries: Exploring prospects of the emerging climate change crisis. *Int. J. Econ. Financ. Stud.* **2020**, *12*, 239–254. [[CrossRef](#)]
- Van Huong, N.; Minh Nguyet, B.T.; Van Hung, H.; Minh Duc, H.; Van Chuong, N.; Do Tri, M.; Van Hien, P. Economic impact of climate change on agriculture: A case of Vietnam. *AgBioForum* **2022**, *24*, 1–12.
- Soylu Pekpostalci, D.; Tur, R.; Danandeh Mehr, A.; Vazifekhah Ghaffari, M.A.; Dąbrowska, D.; Nourani, V. Drought monitoring and forecasting across Turkey: A contemporary review. *Sustainability* **2023**, *15*, 6080. [[CrossRef](#)]
- Tan, Y.X.; Ng, J.L.; Huang, Y.F. A Review on Drought Index Forecasting and Their Modelling Approaches. *Arch. Comput. Methods Eng.* **2023**, *30*, 1111–1129. [[CrossRef](#)]
- Dunn, S.M.; Brown, I.; Sample, J.; Post, H. Relationships between climate, water resources, land use and diffuse pollution and the significance of uncertainty in climate change. *J. Hydrol.* **2012**, *434*, 19–35. [[CrossRef](#)]
- Pirnia, A.; Golshan, M.; Darabi, H.; Adamowski, J.; Rozbeh, S. Using the Mann–Kendall test and double mass curve method to explore stream flow changes in response to climate and human activities. *J. Water Clim. Chang.* **2018**, *10*, 725–742. [[CrossRef](#)]
- Li, F.; Zhang, G.; Xu, Y.J. Spatiotemporal variability of climate and streamflow in the Songhua River Basin, northeast China. *J. Hydrol.* **2014**, *514*, 53–64. [[CrossRef](#)]
- Ghazi, B.; Dutt, S.; Torabi Haghighi, A. Projection of Future Meteorological Droughts in Lake Urmia Basin, Iran. *Water* **2023**, *15*, 1558. [[CrossRef](#)]
- Chang, J.; Wang, Y.; Istanbuluoglu, E.; Bai, T.; Huang, Q.; Yang, D.; Huang, S. Impact of climate change and human activities on runoff in the Weihe River Basin, China. *Quat. Int.* **2015**, *380*, 169–179. [[CrossRef](#)]
- El-Khalifa, Z.S.; Zahran, H.F.; Ayoub, A. Climate Change Factors' Impact on the Egyptian Agricultural Sector. *Asian J. Agric. Rural. Dev.* **2022**, *12*, 192–200. [[CrossRef](#)]
- Chong, K.L.; Huang, Y.F.; Koo, C.H.; Ahmed, A.N.; El-Shafie, A. Spatiotemporal variability analysis of standardized precipitation indexed droughts using wavelet transform. *J. Hydrol.* **2022**, *605*, 127299. [[CrossRef](#)]
- Adu-Prah, S.; Tetteh, E.K. Spatiotemporal analysis of climate variability impacts on malaria prevalence in Ghana. *Appl. Geogr.* **2015**, *60*, 266–273. [[CrossRef](#)]
- Wang, S.; Wang, Y.; Ran, L.; Su, T. Climatic and anthropogenic impacts on runoff changes in the songhua river basin over the last 56 years (1955–2010), Northeastern China. *Catena* **2015**, *127*, 258–269. [[CrossRef](#)]
- Wen, X.; Wu, X.; Gao, M. Spatiotemporal variability of temperature and precipitation in Gansu Province (Northwest China) during 1951–2015. *Atmos. Res.* **2017**, *197*, 132–149. [[CrossRef](#)]
- Danandeh Mehr, A.; Hrnjica, B.; Bonacci, O.; Torabi Haghighi, A. Innovative and successive average trend analysis of temperature and precipitation in Osijek, Croatia. *Theor. Appl. Climatol.* **2021**, *145*, 875–890. [[CrossRef](#)]
- Panditharathne, R.; Gunathilake, M.B.; Chathuranika, I.M.; Rathnayake, U.; Babel, M.S.; Jha, M.K. Trends and Variabilities in Rainfall and Streamflow: A Case Study of the Nilwala River Basin in Sri Lanka. *Hydrology* **2023**, *10*, 8. [[CrossRef](#)]
- Abou Zaki, N.; Torabi Haghighi, A.; Rossi, P.M.; Tourian, M.J.; Bakhshae, A.; Kløve, B. Evaluating impacts of irrigation and drought on river, groundwater and a terminal wetland in the Zayanderud Basin, Iran. *Water* **2020**, *12*, 1302. [[CrossRef](#)]
- Diani, K.; Kacimi, I.; Zemzami, M.; Tabyaoui, H.; Haghighi, A.T. Evaluation of meteorological drought using the Standardized Precipitation Index (SPI) in the High Ziz River basin, Morocco. *Limnol. Rev.* **2019**, *19*, 125–135. [[CrossRef](#)]
- Dabanlı, İ. A climate change impact: Variation in precipitation patterns, and increased drought risk in Turkey. *Sak. Univ. J. Sci.* **2019**, *23*, 193–202. [[CrossRef](#)]
- Altın, T.B.; Sarıç, F.; Altın, B.N. Determination of drought intensity in Seyhan and Ceyhan River Basins, Turkey, by hydrological drought analysis. *Theor. Appl. Climatol.* **2020**, *139*, 95–107. [[CrossRef](#)]

25. Gumus, V.; Simsek, O.; Avsaroglu, Y.; Agun, B. Spatio-temporal trend analysis of drought in the GAP Region, Turkey. *Nat. Hazards* **2021**, *109*, 1759–1776. [[CrossRef](#)]
26. Danandeh Mehr, A.; Vaheddoost, B. Identification of the trends associated with the SPI and SPEI indices across Ankara, Turkey. *Theor. Appl. Climatol.* **2020**, *139*, 1531–1542. [[CrossRef](#)]
27. Eris, E.; Cavus, Y.; Aksoy, H.; Burgan, H.I.; Aksu, H.; Boyacioglu, H. Spatiotemporal analysis of meteorological drought over Kucuk Menderes River Basin in the Aegean Region of Turkey. *Theor. Appl. Climatol.* **2020**, *142*, 1515–1530. [[CrossRef](#)]
28. Mersin, D.; Gulmez, A.; Safari, M.J.S.; Vaheddoost, B.; Tayfur, G. Drought Assessment in the Aegean Region of Turkey. *Pure Appl. Geophys.* **2022**, *179*, 3035–3053. [[CrossRef](#)]
29. Todaro, V.; D’Oria, M.; Secci, D.; Zanini, A.; Tanda, M.G. Climate Change over the Mediterranean Region: Local Temperature and Precipitation Variations at Five Pilot Sites. *Water* **2022**, *14*, 2499. [[CrossRef](#)]
30. Stathi, E.; Kastridis, A.; Myronidis, D. Analysis of Hydrometeorological Trends and Drought Severity in Water-Demanding Mediterranean Islands under Climate Change Conditions. *Climate* **2023**, *11*, 106. [[CrossRef](#)]
31. Mersin, D.; Tayfur, G.; Vaheddoost, B.; Safari, M.J.S. Historical Trends Associated with Annual Temperature and Precipitation in Aegean Turkey, Where Are We Heading? *Sustainability* **2022**, *14*, 13380. [[CrossRef](#)]
32. Haghghi, A.T.; Yaraghi, N.; Sönmez, M.E.; Darabi, H.; Kum, G.; Çelebi, A.; Kløve, B. An index-based approach for assessment of upstream-downstream flow regime alteration. *J. Hydrol.* **2021**, *600*, 126697. [[CrossRef](#)]
33. Sang, Y.F.; Wang, Z.; Liu, C. Comparison of the MK test and EMD method for trend identification in hydrological time series. *J. Hydrol.* **2014**, *510*, 293–298. [[CrossRef](#)]
34. Chen, Z.; Chen, Y.; Li, B. Quantifying the effects of climate variability and human activities on runoff for Kaidu River Basin in arid region of northwest China. *Theor. Appl. Climatol.* **2013**, *111*, 537–545. [[CrossRef](#)]
35. Rosmanna, T.; Domínguez, E.; Chavarro, J. Comparing trends in hydro-meteorological average and extreme data sets around the world at different time scales. *J. Hydrol. Reg. Stud.* **2015**, *5*, 200–212. [[CrossRef](#)]
36. Xu, C.; Li, J.; Zhao, J.; Gao, S.; Chen, Y. Climate variations in northern Xinjiang of China over the past 50 years under global warming. *Quatern. Int.* **2015**, *358*, 83–92. [[CrossRef](#)]
37. Hefzul Bari, S.; Rahman, T.U.; Hoque Azizul, M.; Hussain, M. Analysis of seasonal and annual rainfall trends in the northern region of Bangladesh. *Atmos. Res.* **2016**, *176–177*, 148–158. [[CrossRef](#)]
38. Bărbulescu, A.; Postolache, F. Are the Regional Precipitation and Temperature Series Correlated? Case Study from Dobrogea, Romania. *Hydrology* **2023**, *10*, 109. [[CrossRef](#)]
39. Hayes, M.J.; Svoboda, M.D.; Wihite, D.A.; Vanyarkho, O.V. Monitoring the 1996 drought using the standardized precipitation index. *Bull. Am. Meteorol. Soc.* **1999**, *80*, 429–438. [[CrossRef](#)]
40. Mallya, G.; Mishra, V.; Niyogi, D.; Tripathi, S.; Govindaraju, R.S. Trends and variability of droughts over the Indian monsoon region. *Weather. Clim. Extrem.* **2016**, *12*, 43–68. [[CrossRef](#)]
41. Torabi Haghghi, A.; Abou Zaki, N.; Rossi, P.M.; Noori, R.; Hekmatzadeh, A.A.; Saremi, H.; Kløve, B. Unsustainability syndrome—From meteorological to agricultural drought in arid and semi-arid regions. *Water* **2020**, *12*, 838. [[CrossRef](#)]
42. McCormick, M.; Thomason, L.; Trepte, C. Atmospheric effects of the Mt Pinatubo eruption. *Nature* **1995**, *373*, 399–404. [[CrossRef](#)]
43. Çuhadar, M.; Atiş, E. Drought Analysis in Ceyhan Basin Using Standardized Precipitation Index. *J. Inst. Sci. Technol.* **2019**, *9*, 2303–2312. [[CrossRef](#)]

Disclaimer/Publisher’s Note: The statements, opinions and data contained in all publications are solely those of the individual author(s) and contributor(s) and not of MDPI and/or the editor(s). MDPI and/or the editor(s) disclaim responsibility for any injury to people or property resulting from any ideas, methods, instructions or products referred to in the content.